ELSEVIER

Journal of Power Sources 112 (2002) 67–75

JOURNAL OF POWER SOURCES

www.elsevier.com/locate/jpowsour

Effect of platinum co-sputtering on characteristics of amorphous vanadium oxide films

Han-Ki Kim[a], Tae-Yeon Seong[a], Young Soo Yoon[b,*]

[a]*Department of Materials Science and Engineering, Kwangju Institute of Science and Technology (K-JIST), Kwangju 500-712, South Korea*

[b]*Thin Film Technology Research Center, Korea Institute of Science and Technology (KIST), P.O. Box 131 Choengryang, Seoul 130-650, South Korea*

Received 10 April 2002; accepted 10 June 2002

Abstract

The effect of platinum co-sputtering on the characteristics of amorphous V_2O_5 films, grown by dc reactive sputtering, is investigated. The co-sputtering process influences the growth mechanism as well as the characteristics of the V_2O_5 films. Glancing-angle X-ray diffraction (GXRD), transmission electron microscopy (TEM), and Fourier transform infrared (FT-IR) results indicate that the microstructure of the V_2O_5 films is affected by the rf power of the co-sputtered platinum. In addition, it is found that the platinum co-sputtered V_2O_5 cathode film exhibits better cycleability than an undoped V_2O_5 cathode film. This is due to the absence of short-range order, which is generally present in undoped V_2O_5 cathode films. Possible explanations are given to describe the dependence of the cycleability V_2O_5 films on the platinum rf power and the growth mechanism of the V_2O_5 film.

Keywords: Platinum co-sputtering; V_2O_5; Cycleability; Micro-power source; Short-range order; Thin-film battery

1. Introduction

Due to successes in the development of microelectronic mechanical systems (MEMS) and micro-devices, the fabrication of high-quality micro-power sources, such as thin-film batteries (TFBs) and thin-film supercapacitors (TFSCs) is of great technological importance [1–5]. Because a TFB has a unique advantage, in that it can be imcorporated into the same integrated circuit with other electronic elements, it has great potential for use in areas such as smart cards, on-chip power sources, and portable electronic devices.

A variety of oxide films, such as $LiCoO_2$, $LiNi_{1-x}Co_xO_2$, $LiMn_2O_4$, and V_2O_5 are potential cathode materials for use in a thin-film microbattery [6–10]. Among these oxide materials, V_2O_5 is particularly promising due to its unique isotropic structure and faster ion channels, high specific energy, and ease of preparation [3,10,11]. In particular, conventional annealing processes, typically used in $LiMO_2$ systems (M = Ni, Co, and Mn), are not required for amorphous V_2O_5. As a result, amorphous V_2O_5 could be used as a cathode film in on-chipped thin-film microbatteries. In order to improve the electrochemical properties of the V_2O_5, several workers have employed alloying or doping processes. Recently, Coustier et al. [12] investigated both copper and silver-doped vanadium oxide, and reported that the electronic conductivity of V_2O_5 was increased two- to three-fold by such doping. The gel type copper- or silver-doped V_2O_5 samples are not suitable, however, for the fabrication of thin-film microbatteries. Therefore, it is imperative to develop suitable doping or co-sputtering processes, which can modify the characteristics of a cathode film, for use in the fabrication of thin-film microbatteries. Although some research groups have studied doping or alloying effects on V_2O_5 films [13], most research has focused the electrochemical properties of such films. In order to grow amorphous V_2O_5 with good cycleability, it is very important to obtain a better understanding of the growth mechanism and characteristics of co-sputtered cathode films.

In this study, we evaluate the effect of platinum co-sputtering on the electrochemical, structural, chemical

Abbreviations: AFM, atomic force microscopy; FT-IR, Fourier transform infrared spectroscopy; GXRD, glancing-angle X-ray diffraction; RBS, Rutherford backscattering spectroscopy; SEM, scanning electron microscopy; TED, transmission electron detection; TEM, transmission electron microscopy

* Corresponding author. Tel.: +82-2-958-5558; fax: +82-2-957-6851.
E-mail address: ysyoon@kist.re.kr (Y.S. Yoon).

0378-7753/02/$ – see front matter
PII: S0378-7753(02)00343-9

and surface properties of amorphous V_2O_5 films grown on Pt–Ti–Si substrates by dc reactive magnetron sputtering. Based on Rutherford backscattering spectroscopy (RBS), TEM, glancing-angle X-ray diffraction (GXRD), transmission electron diffraction (TED), Fourier transform infrared spectroscopy (FT-IR), scanning electron microscopy (SEM), atomic force microscopy (AFM) and electrochemical results, a possible mechanism for enhancing the cycleability of a V_2O_5 cathode film by platinum co-sputtering is proposed.

2. Experimental

Amorphous V_2O_5 (a-V_2O_5) cathode films were deposited on Pt–Ti–Si substrates by means of a specially designed, dual-target, magnetron dc sputtering system using a pure vanadium metal target (99.99% Super Conductor Inc.) at room temperature. The platinum film (300 nm thick), acting as a current-collector, was grown on to the titanium adhesive layer by dc sputtering using a pure platinum metal target (99.99% Super Conductor Inc.). The a-V_2O_5 films were then grown over the platinum current-collector by means of a dc reactive sputtering system using a vanadium target at a power of 370 W. The a-V_2O_5 films were simultaneously co-sputtered with a high-purity metal platinum target at an rf power which ranged from 0 to 50 W. For simplicity, a V_2O_5 film co-sputtered at an rf power of 10 W is referred to as 'a 10 W V_2O_5 film', and so on. A schematic of the co-sputtering system used to deposit a-V_2O_5 or platinum co-sputtered V_2O_5 films is shown in Fig. 1. The base pressure in the chamber was 2×10^{-6} Torr and the working pressure was maintained constant at 5 m Torr during the deposition. The extent of platinum incorporation into the V_2O_5 cathode film was characterized by Rutherford backscattering spectrometry (RBS: NEC 6SDH-2). After film deposition, half-cell structures were fabricated to analyze the electrochemical properties of the as-deposited vanadium films. The anode and electrolyte were pure lithium metal and polypropylene with liquid 1 M $LiPF_6$ (EC:DMC = 1:1), respectively. The room temperature charge–discharge property based on a half-cell with constant current of 50 μA cm^{-2} was measured by a cycler (Wonatech com. WBCS300) between 3.6 and 2.2 V. Fourier transform infrared (FT-IR: Polaris^{TM} Mattson) was employed to investigate the chemical binding states of V_2O_5 with increasing platinum rf power. The surface morphology change of the V_2O_5 film with increasing Pt rf power was examined by scanning electron microscopy (SEM: Hitachi 4-4100) and atomic force microscopy (AFM: PSIA). The microstructure of the undoped and platinum co-sputtered V_2O_5 films was examined by GXRD (Rigaku diffractometer: D/MAX-RC) and HREM (JEM 2010) operated at 200 kV. Cross-section, thin-foil specimens for electron microscopy examination were prepared using standard procedures and finished by Ar^+ ion thinning with the specimens cooled to ~77 K.

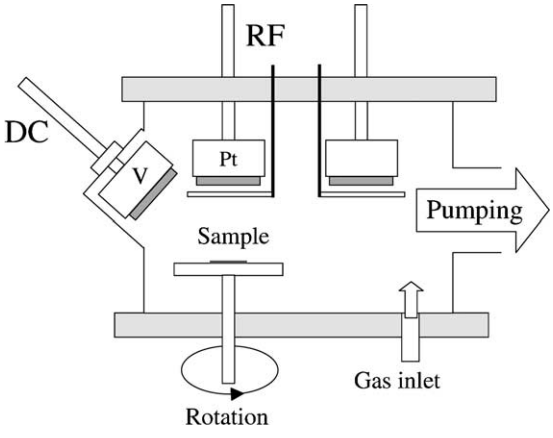

Fig. 1. Schematic figure of rf and dc sputtering system used for platinum co-sputtering.

3. Results and discussion

The growth rate of a-V_2O_5 film with increasing platinum rf power from 0 to 50 W is shown in Fig. 2. The platinum co-sputtering with 10 and 30 W rf power resulted in a remarkable decrease in growth rate to half that of an undoped V_2O_5 film. Increasing the platinum rf power to 50 W led to an increase in the growth rate up to 21 Å min^{-1}. Thus, it appears that different mechanisms are involved in the growth of a-V_2O_5 with increasing platinum rf power, which result in a variation of growth rate. The composition of the undoped and platinum co-sputtered V_2O_5 films was determined from RBS analysis. The composition of platinum in the V_2O_5 is $Pt_{0.01}V_2O_{4.76}$, $Pt_{0.72}V_2O_{4.73}$ and $Pt_{2.27}V_2O_{4.78}$ for the 10-, 30- and 50-W V_2O_5 films, respectively. Compared with the 30- and 50-W V_2O_5 films, the 10-W V_2O_5 film shows a lower level of platinum atoms, which is similar to that of

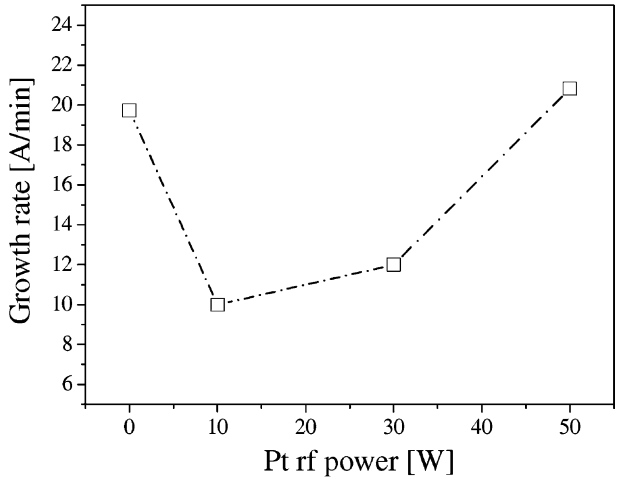

Fig. 2. Growth rate of V_2O_5 films with increasing platinum rf power co-sputtering with low rf power (10 and 30 W reduces remarkably the growth rate of V_2O_5 film.

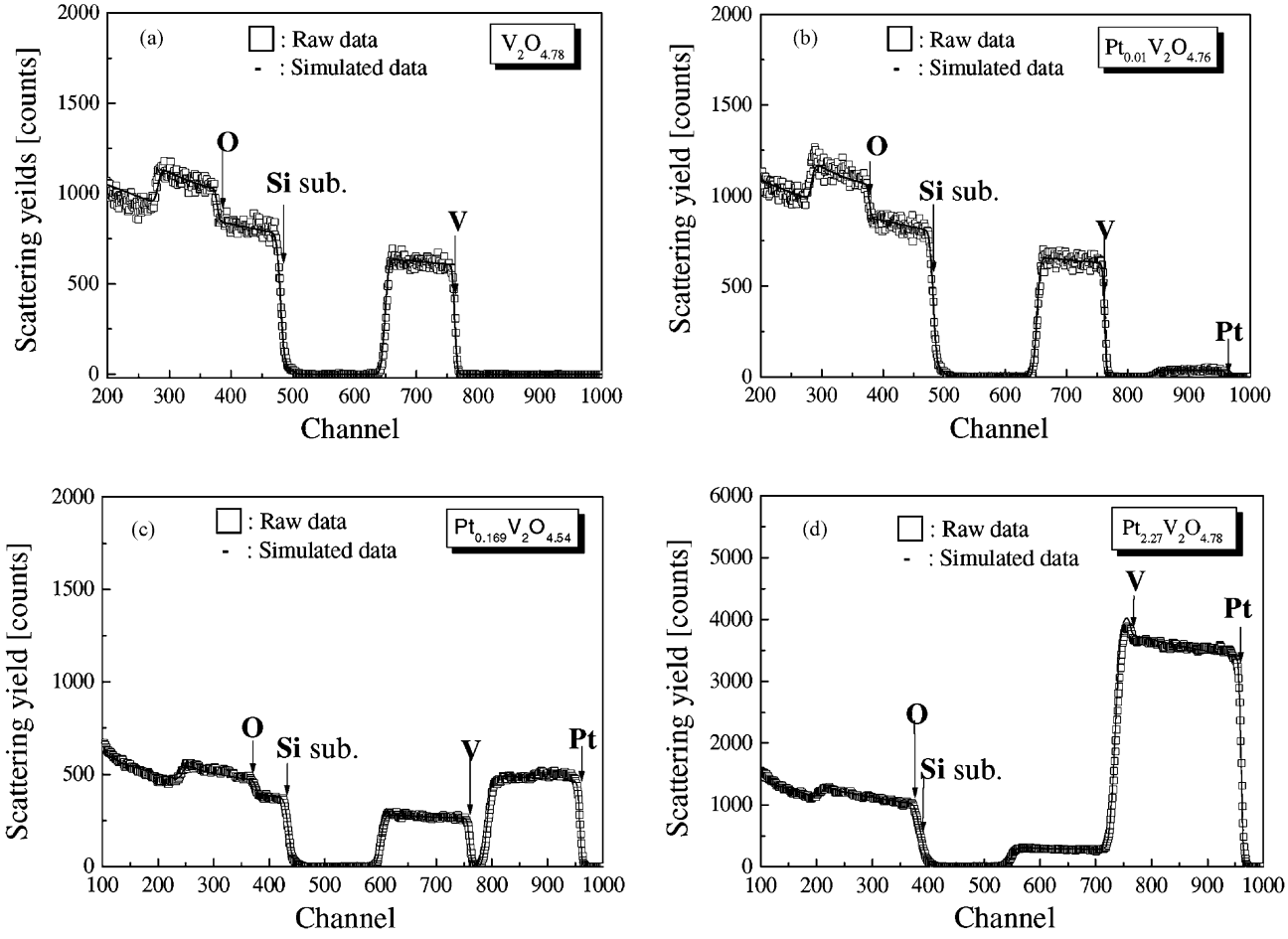

Fig. 3. RBS spectrum for (a) undoped, (b) 10-W, (c) 30-W, and (d) 50-W platinum sputtered V_2O_5 films on silicon substrate. Continuous line is calculated backscattering.

undoped films, as shown in Fig. 3. These results indicate that a 10-W platinum co-sputtered V_2O_5 film can be legitimately characterized as doped V_2O_5. Similar behaviour was observed with an Auger electron spectroscopy investigation (AES) of depth profile analysis (not shown).

To investigate the dependence of platinum co-sputtering on the electrochemical properties of the V_2O_5 films, a half-cell was fabricated with the configuration; Li polypropylene with liquid 1 M $LiPF_6$ (EC:DMC = 1:1)/V_2O_5/Pt/Ti–Si. The specific discharge capacities of the platinum co-sputtered V_2O_5 films at different rf power are shown in Fig. 4 as a function of cycle number. The cells were cycled between 3.6 and 2.2 V at a constant density of 50 μA cm^{-2} (the area of all V_2O_5 cathode films was 1.44 cm^2). It is clearly seen that the platinum co-sputtered V_2O_5 films exhibit better cycleability, compared with the undoped film (a-V_2O_5). For the undoped sample, the capacity is drastically degraded with increasing cycle number. For the 10 W V_2O_5, however, the specific capacity is degraded slowly with increasing cycle number. In other words, after 500 cycles, the capacity drops by ∼70 and ∼20% of the initial value for the undoped and 10 W V_2O_5 film, respectively. Although the cycleability of 30- and 50-W V_2O_5 films is inferior to that of 10-W V_2O_5, the performance of the formes two films is superior to that of undoped V_2O_5.

The discharge curve for the first and 500th cycle for undoped and platinum co-sputtered V_2O_5 films are given

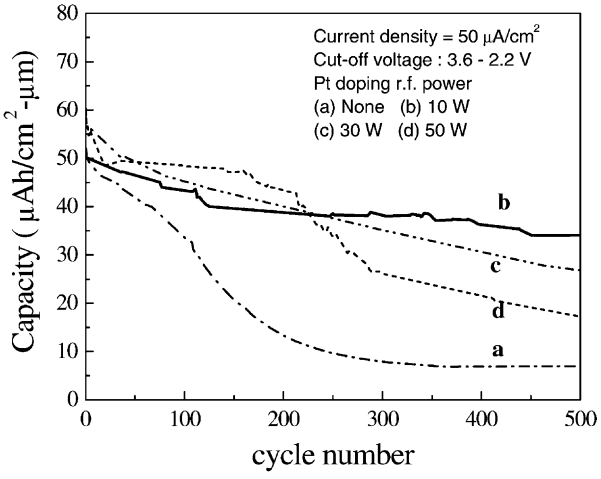

Fig. 4. Discharge capacities of differently doped a-V_2O_5 films cycled between 2.2 and 3.2 V as function of cycle number.

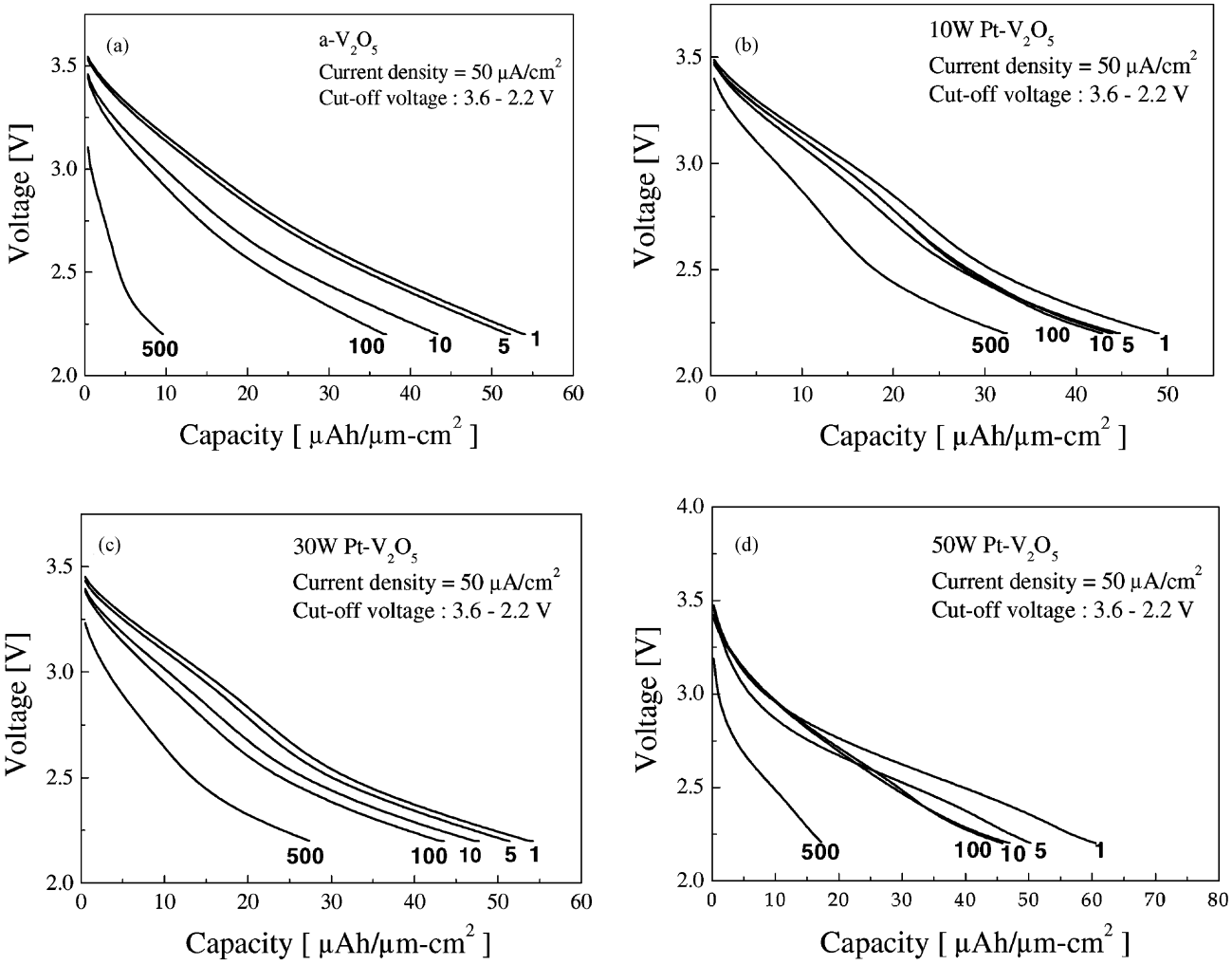

Fig. 5. Discharge curves of undoped and platinum co-sputtered V_2O_5 films measured at 1, 5, 10, 100, and 500 cycles with constant current density of 50 μA cm^{-2}: (a) undoped, (b) 10-W, (c) 30-W, and (d) 50-W platinum co-sputtered V_2O_5 films.

in Fig. 5. Even though all samples show amorphous characteristics with no plateau, a dependence of cycleability on platinum rf power is clearly evident. The discharge curve of 10-W Pt V_2O_5 displays the least capacity fade among the platinum co-sputtered samples. This indicates that dilute platinum co-sputtering (10 W or 30 W) could be used to improve the cycleability of V_2O_5 films, while high power co-sputtering above the doping level degrades the cycleability of samples. For undoped V_2O_5, however, a drastic capacity fade from 55 μAh μm^{-1} cm^{-2} on the first discharge to 10 μAh μm^{-1} cm^{-2} on the 500th discharge is observed. Although the initial capacity of undoped V_2O_5 is higher than that of each platinum co-sputtered sample, a faster capacity fade with increasing cycle number is a distinct disadvantages with the undoped sample. In a previous studies [10,14,15], we showed that an amorphous vanadium oxide film without short-range order can be obtained by the platinum doping process. Therefore, it is possible that the electrochemical characteristics of the V_2O_5 film can be changed via structural modification of the cathode film, which can be effected by a platinum co-sputtering process.

The FT-IR absorption bands for V_2O_5 films deposited with increasing platinum rf power are presented in Fig. 6. All samples show broadened absorption bands, which are characteristic of a random structure with a wide distribution of the V–O bond length and angle. By comparison with crystalline V_2O_5 (V=O band: 1020 cm^{-1} and V–O band: 820, 600, 500 cm^{-1}), the broadened peaks, which indicate double bond V=O vibration around 1000 cm^{-1} and V–O vibration around 800 and 600 cm^{-1}, remain in the amorphous state. As shown in the FT-IR spectra, an increase in platinum rf power reduces the intensity of the band at 1000 cm^{-1}. In addition, the V_2O_5 samples, except for 50-W V_2O_5, have similar bonding characteristics, including V=O and V–O bonding. For the 50-W V_2O_5 sample, a shift in the absorption band at 1000 cm^{-1} to a higher wave number is observed. This shift is different to that reported by Yamaki and co-workers [16,17] for V_2O_5 with P_2O_5 and TeO_2 dopants. These authors showed that the V=O band was shifted to a lower wave number, while the other V–O peaks moved to a higher wave number with increasing P_2O_5 content. It was suggested that these shifts were caused by

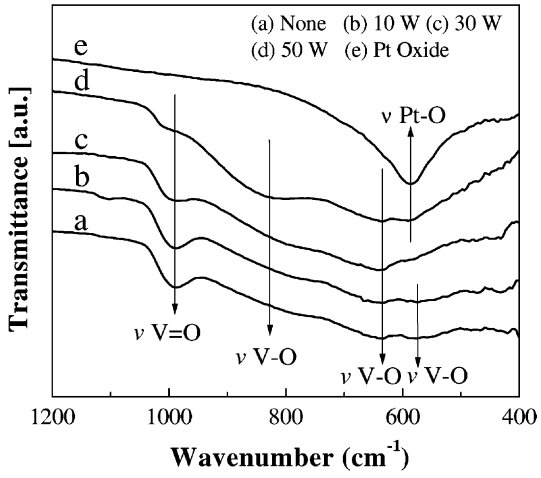

Fig. 6. FT-IR spectra of V_2O_5 films with increasing platinum rf power.

microstructural changes in the V_2O_5 sample from a crystalline to an amorphous structure. Therefore, the different band shifting of the 50-W platinum co-sputtered V_2O_5 film indicates the presence of very small microcrystalline regions in the amorphous V_2O_5 matrix. In addition to the shift in the V=O absorption band, a Pt–O absorption band is present at about 570 cm^{-1}. This absorption band suggests that co-sputtered platinum atoms in the V_2O_5 at a 50-W rf power are present in an amorphous phase or/and a crystalline PtO phase. Therefore, the incorporation of a large amount of platinum atoms into V_2O_5 film result in the formation of microcrystalline structures, such as semiconducting PtO_2 or PtO phases, in amorphous V_2O_5 matrix.

In order to examine the dependence of co-sputtering on the microstructure of the V_2O_5 films, a GXRD analysis was performed; the results are shown in Fig. 7. The GXRD plots of the undoped and platinum co-sputtered films show the characteristic diffraction peaks of the (1 1 1) and (2 0 0) current-collector film on the Ti–Si substrate. In addition, the GXRD plots for all the V_2O_5 films show an additional broad peak ($2\theta = 13.01°$), which is identified as amorphous V_2O_5.

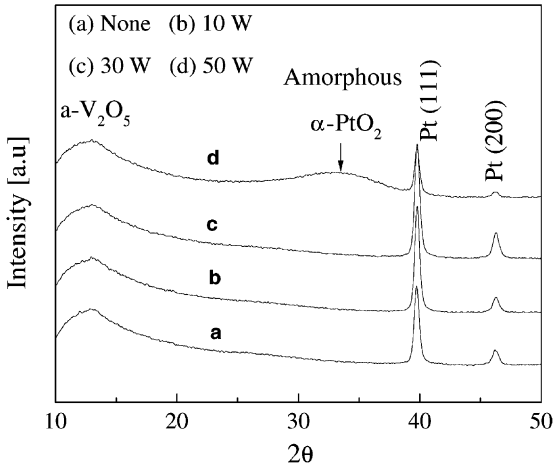

Fig. 7. Glancing angle X-ray diffraction plots of V_2O_5 films.

This indicates that both undoped and Pt co-sputtered films consist of an amorphous V_2O_5 phase. The GXRD structural details of the films doped at rf powers of 10 and 30 W are fairly similar to that of the undoped sample. For the film doped at 50 W, however, an additional broad peak ($2\theta = 33.32°$) is present and is assigned to a PtO_2 phase. This result is consistent with the FT-IR results, as shown in Fig. 6.

The dependence of platinum co-sputtering on the microstructures of the V_2O_5 films was further investigated by HREM and TED measurements. Cross-sectional HREM images obtained from the interface regions including platinum layers and V_2O_5 films, are given in Fig. 8. The HREM image of the undoped sample reveals an amorphous feature (Fig. 8(a)), which is consistent with the GXRD result (Fig. 7).

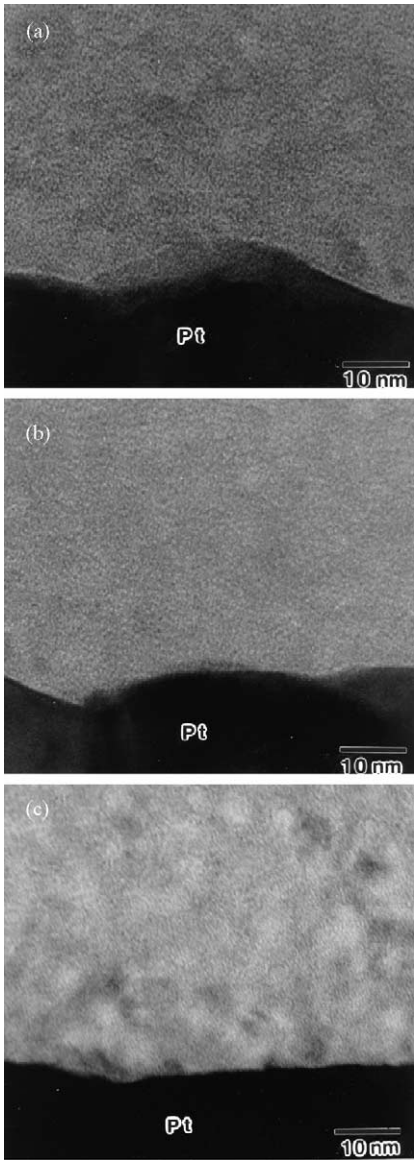

Fig. 8. Cross-sectional HREM images obtained from interface regions including platinum layers and V_2O_5 films; (a) undoped, (b) 10-W, and (c) 30-W platinum co-sputtered samples.

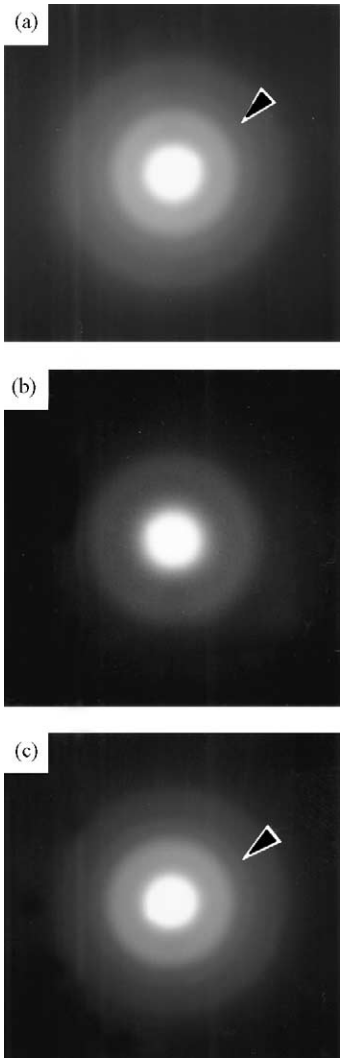

Fig. 9. TED patterns for (a) undoped, (b) 10-W doped, and (c) 30-W doped V_2O_5 films. A very weak diffuse ring indicated by arrows in undoped and 30-W V_2O_5 films indicates films have some short-range order. For 10-W V_2O_5 film, however, there is no extra diffuse ring.

A TED pattern obtained from the undoped sample (Fig. 9(a)) exhibits diffuse ring patterns, which are characteristic of an amorphous material. In addition, a very weak diffuse ring can be seen, as indicated by the arrow. This diffracted feature indicates that the undoped V_2O_5 film is not completely amorphous, but has some short-range order. A similar structure was observed in V_2O_5 xerogel films [18,19]. Based on XRD results, Aldebert et al. [18] and Legendre and Livage [19] reported that spin-coated V_2O_5 films were amorphous with short-range order and consist of self-aligned, ribbon-like fibres. For the 10-W V_2O_5 film (Fig. 8(b)), the HREM image shows a very uniform amorphous contrast. A TED pattern of the 10-W V_2O_5 film reveals diffuse ring patterns (Fig. 9(b)), which is characteristic of amorphous materials. It is noteworthy that, unlike the undoped sample, extra diffuse ring is not present for this sample. This indicates that the 10-W V_2O_5 film is completely amorphous and contains no short-range order structure. Thus, the addition of a small amount of platinum can play a substantial role in randomizing the short-range ordered V_2O_5. For the film doped at 30 W (Fig. 8(c)), however, the HREM image reveals a somewhat non-uniform contrast, compared with the image for the 1–30-W film. A TED pattern for the 30-W V_2O_5 film shows that, in addition to the characteristic amorphous ring patterns, a weak extra diffuse ring (Fig. 9(c)) is present, as indicated by the arrow. This diffracted ring is the same as that for the undoped sample, which implies that a feature related to range order is formed again in the 30-W V_2O_5 film. An HREM image obtained from the 50-W V_2O_5 film is given in Fig. 10. There is a high density of dark blobs from ~1 to ~3 nm across. It should be noted that in addition to the dark blobs, nanocrystallites are also present. The inset in Fig. 10 shows a TED pattern for the 50-W V_2O_5 film. His clearly seen that, in addition to the characteristic features similar to those for the 30-W V_2O_5 film, an extra diffuse ring containing small-diffracted spots is present. This is indicative of the presence of amorphous and crystalline phases. The enlarged image of a 50-W V_2O_5 film in Fig. 11 displays the embedded microcrystalline structure in the V_2O_5 matrix. These crystallites typically range from ~1.2 to ~4 nm in size and are believed to be PtO_2 crystallites. The GXRD, HREM and TED results show that the 50-W V_2O_5 film consists of three different phases, namely, amorphous V_2O_5 with some short-range order, amorphous PtO_2, and crystalline PtO_2. The dark blobs in the inset of Fig. 10 are thought to be contrast associated with these three phases. The HREM and TED results indicate that as the platinum content is increased, the cathode films undergo structural changes from an amorphous structure, to an amorphous structure with short-range order, and then to an amorphous structure with short-range order containing amorphous and crystalline PtO_2 phases. Yu et al. [20] investigated the effects of doping on the kinetics of the solid-phase growth of amorphous alumina films on sapphire. They showed that the introduction of dopants (Cr and Fe) could modify the growth rate. If the addition of platinum and/or PtO_2 could affect the growth of V_2O_5 films, Then a modified growth behaviour might be responsible for the occurrence of the different microstructures.

The change in surface morphology with increasing platinum rf power was examined by SEM and AFM analysis. Electron micrographs of V_2O_5 grown on the Pt/Ti–Si substrate with increasing platinum rf power are presented in Fig. 12. The surface of the undoped V_2O_5 film (Fig. 12(a)) is smoother than that of the platinum doped samples. Furthermore, increase in the platinum rf power is found to lead to an increase in surface morphology of the platinum co-sputtered V_2O_5 films. In particular, the 50-W film has a larger cluster shape with a higher root mean square (RMS) roughness of 72 K, compared and with the undoped (35 Å) and 30-W (41 Å) samples.

The previous results indicate that the platinum co-sputtering process affects the electrochemical, microstructural,

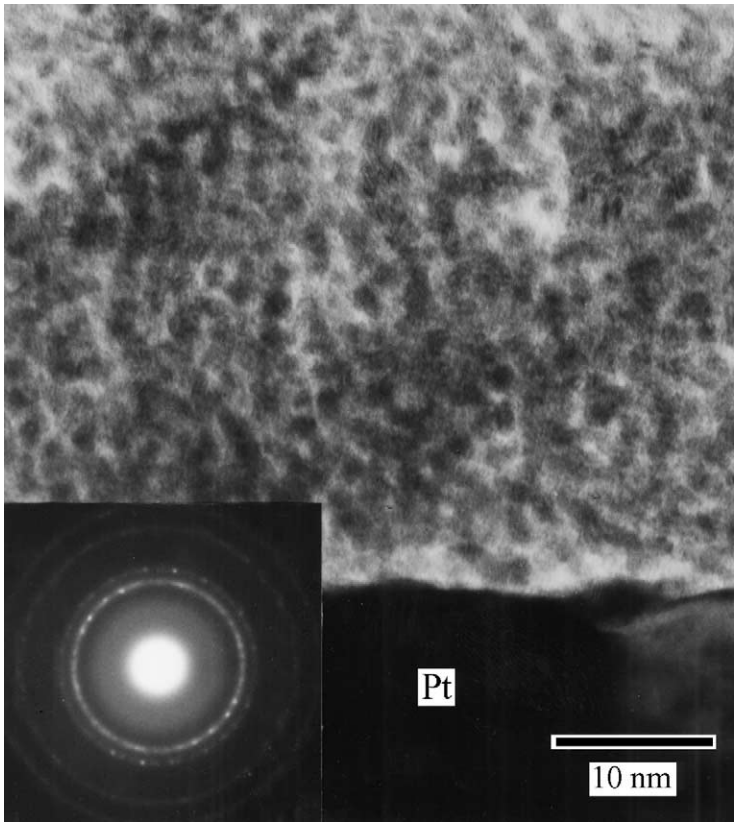

Fig. 10. Cross-sectional HREM image of 50-W V_2O_5 film with inset showing TED pattern.

surface, and chemical properties of V_2O_5 films. This behaviour can be attributed to microstructural changes in V_2O_5 films as a result of the platinum co-sputtering process. This microstructural change is caused by change in growth mechanism during platinum co-sputtering. A schematic diagram of the effect of platinum co-sputtering on the growth mechanism given Fig. 13. During reactive sputtering in oxygen, large numbers of negative oxygen ions are present. A fraction of these oxygen ions will be accelerated in the space charge field and will be directed towards the growing V_2O_5 film, and in an opposite direction to the positively changed argon ions. As the platinum is co-sputtered to the growing film, the V_2O_5 layer contains some platinum in addition to V and O atoms. When a small concentration of a heavy element (atomic weight of Pt = 195) is added to a lower mass element (V = 51), a sputtering yield amplification effect (SYA), which was observed by Berg and Katardjiev [21], will occur, as shown in Fig. 13(a). The result of this effect is that the re-sputtering yield of the lower mass element may increase significantly. Therefore, the net-growth rate of the 10- and 30-W V_2O_5 films, as shown in Fig. 2, is considerably lower than that of undoped V_2O_5 film. Furthermore, the energetic bombardment by negative oxygen ions of the V_2O_5 film could assist in the amorphization of the V_2O_5 film, as shown in TEM analysis. Therefore, the improved cycleability of 10 and 30 W V_2O_5 cathode films could be related to microstructural changes induced by the platinum co-sputtering process. As the platinum rf power is increased, however, some of the platinum may start to shadow part of the V_2O_5 film and therefore present it from being bombarded by energetic negative oxygen ions. In a collision, a platinum atom at the surface of the growing V_2O_5 film can easily reflect an energetic oxygen ion, as shown in Fig. 13(b). This may also explain why a PtO_2 microcrystalline phase begins to appear at higher platinum concentration. Another reason for improving cycleability by platinum co-sputtering may be

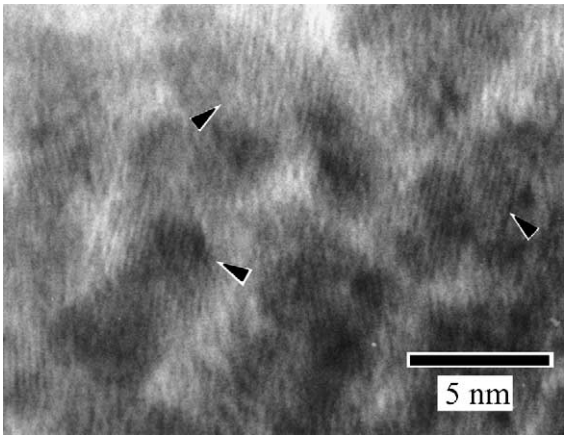

Fig. 11. Enlarged HREM image of 50-W V_2O_5 film. In addition to dark blobs, nanocrystallites are present, as indicated by arrows.

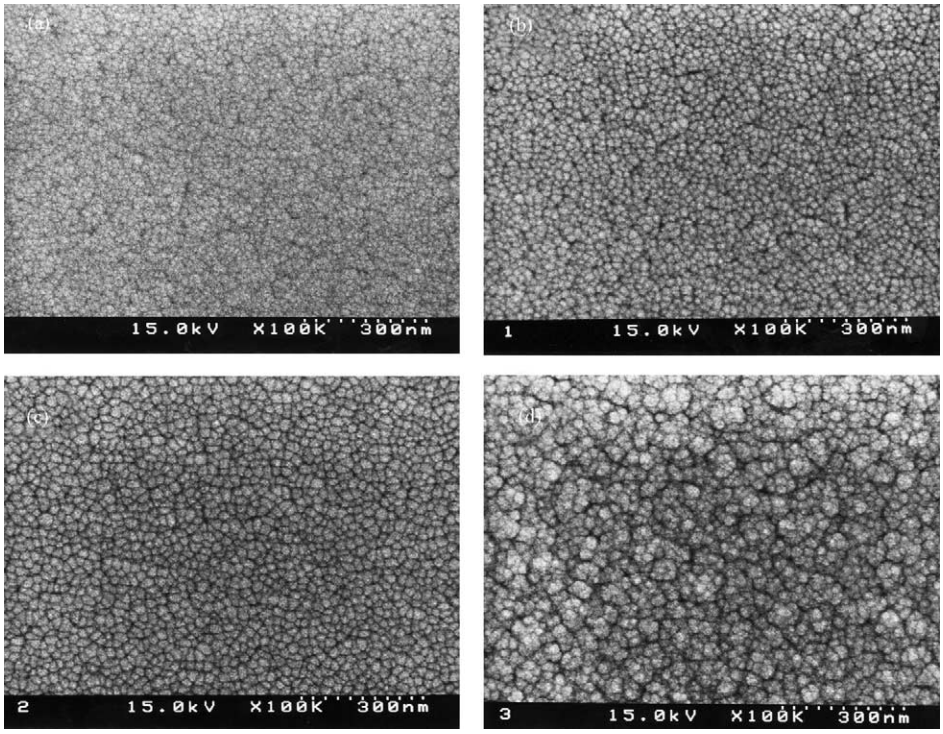

Fig. 12. SEM surface images of the V_2O_5 films with increasing Pt rf power: (a) undoped, (b) 10 W, (c) 30 W, and (d) 50 W Pt co-sputtered V_2O_5 films.

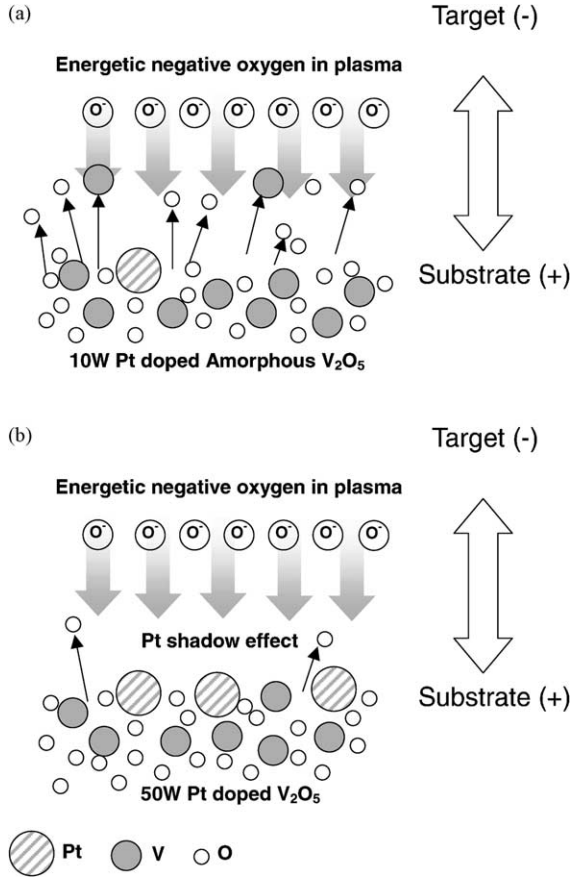

Fig. 13. Different growth mechanisms for (a) 10 W and (b) 50 W Pt co-sputtered V_2O_5 films. A dilute doping of a heavy mass atom results in a resputtering yield amplification effect.

volume buffering effects due to the presence of platinum and/or PtO_2 crystallites. The a-V_2O_5 cathodes can, undergo volume expansion during the lithium insertion–extraction process. The uniformly dispersed platinum and PtO_2 crystallites could suppress this volume expansion which could be a main cause of degradation of the reversibility of lithium intercalation, and consequently give rise to an improved performance.

Therefore, the enhanced cycleability of a platinum co-sputtered V_2O_5 cathode film is attributed to the combined effects of a random structure without short-range order caused by the platinum co-sputtering process and the result of platinum buffering effects.

4. Conclusions

The effect of platinum co-sputtering on V_2O_5 films has been investigated using GXRD, TEM, TED, RBS, FT-IR, AFM, and SEM. It is found that the platinum co-sputtered samples exhibit better cycleability than undoped ones, due to a change in microstructure. In particular, a 10-W platinum co-sputtered V_2O_5 film shows a remarkably improved cycleability. From HREM results, it is observed that the platinum co-sputtering process with 10-W rf power results in a completely amorphous V_2O_5 film without short-range order, which is shown in undoped V_2O_5 and 30-W V_2O_5 samples. This indicates that there is a close relationship between the cycleability and microstructure of the V_2O_5 cathode. In addition, a possible mechanism for the effect of platinum co-sputtering on the V_2O_5 films is suggested.

Acknowledgements

This work was partly supported by the Brain Korea 21 project. One of the authors (H.-K. Kim) gratefully acknowledges the useful discussion with Professor S. Berg of Uppsala University, Sweden.

References

[1] K. Shokoohi, J.M. Tarascon, B.J. Wilkens, Appl. Phys. Lett. 59 (1991) 1260.
[2] N.J. Dudney, J.B. Bates, R.A. Zuhr, S. Young, J.D. Robertson, H.P. Jun, S.A. Hackney, J. Electrochem. Soc. 146 (1999) 2455.
[3] E.J. Jeon, Y.W. Shin, S.C. Nam, W.I. Cho, Y.S. Yoon, J. Electrochem. Soc. 184 (2001) A318.
[4] H.-K. Kim, T.-Y. Seong, J.-H. Lim, W.I. Cho, Y.S. Yoon, J. Power Sources 102 (2001) 167.
[5] J.H. Lim, D.J. Choi, H.-K. Kim, W.I. Cho, Y.S. Yoon, J. Electrochem. Soc. 148 (2001) A278.
[6] B. Wang, J.B. Bates, F.X. Hart, B.C. Sales, R.A. Zuhr, D.J. Robertson, J. Electrochem. Soc. 143 (1996) 3203.
[7] S.-J. Lee, J.-K. Lee, D.-W. Kim, H.-K. Baik, S.-M. Lee, J. Electrochem. Soc. 143 (1996) L268.
[8] H.-K. Kim, T.-Y. Seong, W.I. Cho, Y.S. Yoon, J. Power Sources 109 (2002) 178.
[9] N.J. Dudney, J.B. Bates, R.A. Zuhr, S. Young, J.D. Robertson, H.P. Jun, S.A. Hackney, J. Electrochem. Soc. 146 (1999) 2455.
[10] H.-K. Kim, O.-W. Ok, T.-Y. Seong, E.J. Jeon, W.I. Cho, Y.S. Yoon, J. Vac. Sci. Technol. A 19 (5) (2001) 2549.
[11] J.B. Bates, G.R. Gruzalski, N.J. Dudney, C.F. Luck, X.-H. Yu, S.D. Jones, Solid State Technol. 59 (1993) 56.
[12] F. Coustier, J. Hill, B. Owens, S. Passerini, W. Smyrl, J. Electrochem. Soc. 146 (1999) 1355.
[13] Y.C. Lim, S.C. Nam, H. Y Park, S. Yoon, W.I. Cho, B.W. Cho, H.S. Jeon, K.S. Yoon, J. Kor. Electrochem. Soc. 3 (2000) 219.
[14] H.-K. Kim, E.J. Joen, Y.-W. Ok, T.-Y. Seong, W.I. Cho, Y.S. Yoon, J. Korea Inst. Elec. Electron. Mater. Eng. 13 (2000) 751.
[15] H.-K. Kim, T.-Y. Seong, E.J. Jeon, W.I. Cho, S. Yoon, J. Kor. Ceram. Soc. 38 (1) (2001) 100.
[16] Y. Sakurai, J. Yamaki, J. Electrochem. Soc. 135 (1988) 791.
[17] T. Hirai, S. Okada, J. Yamaki, J. Electrochem. Soc. 136 (1989) 3163.
[18] P. Aldebert, N. Baffler, N. Gharbi, J. Livage, Mater. Res. Bull. 16 (1981) 669.
[19] J. Legendre, I. Livage, J. Coll. Interface Sci. 94 (1983) 75.
[20] N. Yu, T.W. Simpson, P.C. Mcintyre, M. Nastasl, l.V. Mitchell, Appl. Phys. Lett. 67 (1995) 924.
[21] S. Berg, I. Katardjiev, Surf. Coatings Technol. 84 (1996) 353.